Supporting Information

Chitosan-*grafted*-Poly($_L$-lysine) Dendrons Assisted Facile Self-Assembly of Au Nanoclusters for Enhanced X-Ray Computer Tomography Imaging and Precise MMP-9 Plasmid shRNA Delivery

Siming Yu[1,#,], Rong Wen[1,#], Haiyang Wang[1], Yongchao Zha[1], Lin Qiu[2], Bo Li[1], Wei Xue[1,2,*], Dong Ma[1,*]*

[1] Key Laboratory of Biomaterials of Guangdong Higher Education Institutes, Guangdong Provincial Engineering and Technological Research Center for Drug Carrier Development, Department of Biomedical Engineering, Jinan University, Guangzhou 510632, China

[2] The First Affiliated Hospital of Jinan University, Guangzhou 510632, China

* Corresponding authors: Siming Yu (siming_yu@hotmail.com); Wei Xue (weixue_jnu@hotmail.com); Dong Ma (tmadong@jnu.edu.cn)

[#] These authors contributed equally to this work.

Figure S1. Schematic illustration of the copper catalyzed azide-alkyne cyclization reaction route of CPL dendrons. Synthesis of CS-N_3 (A), alkynyl-PLLD-G_3 (B) and CPL (C).

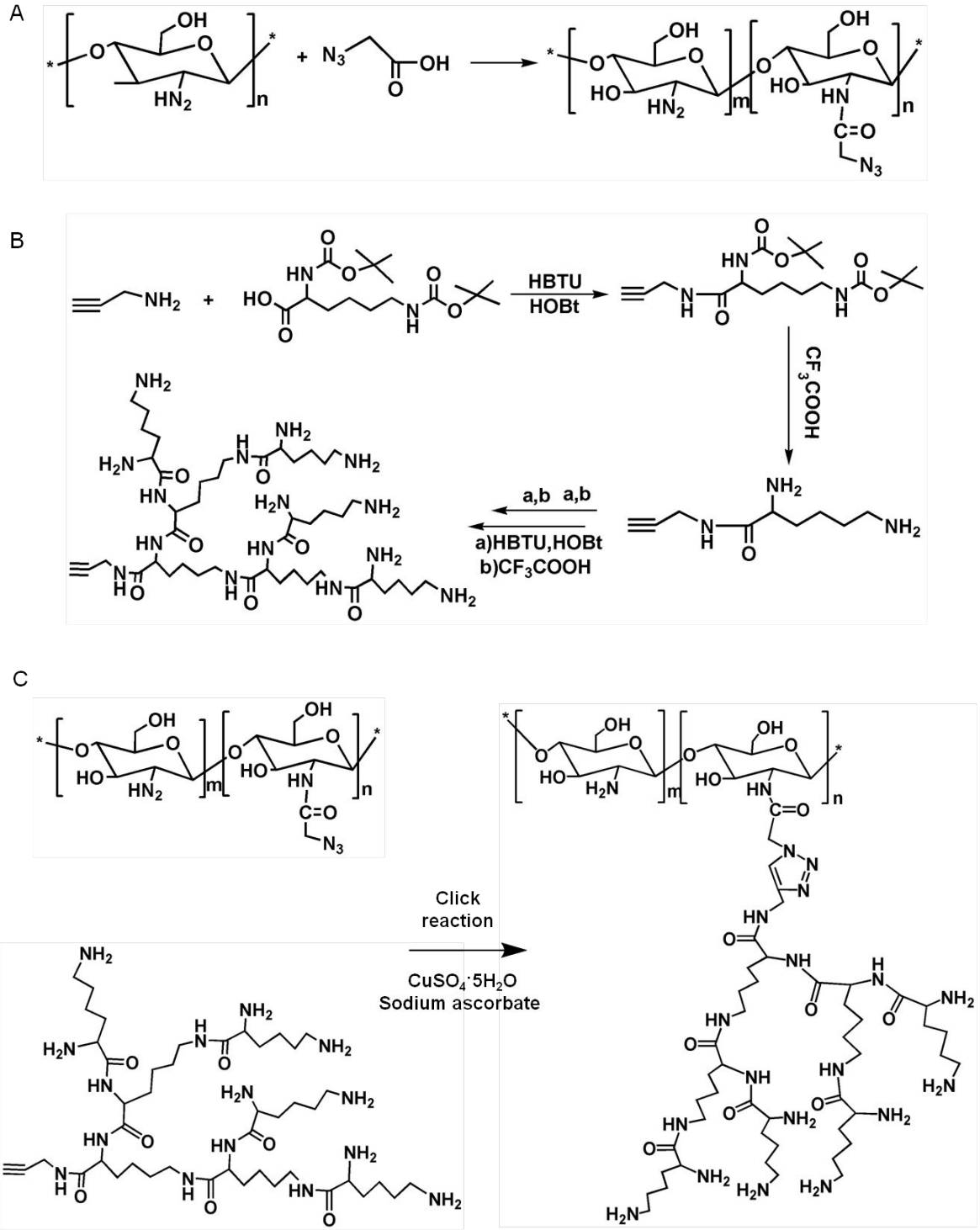

Figure S2. ^{1}H NMR spectra for CS-N_3 (A), alkynyl-PLLD-G_3 (B) and CPL (C).

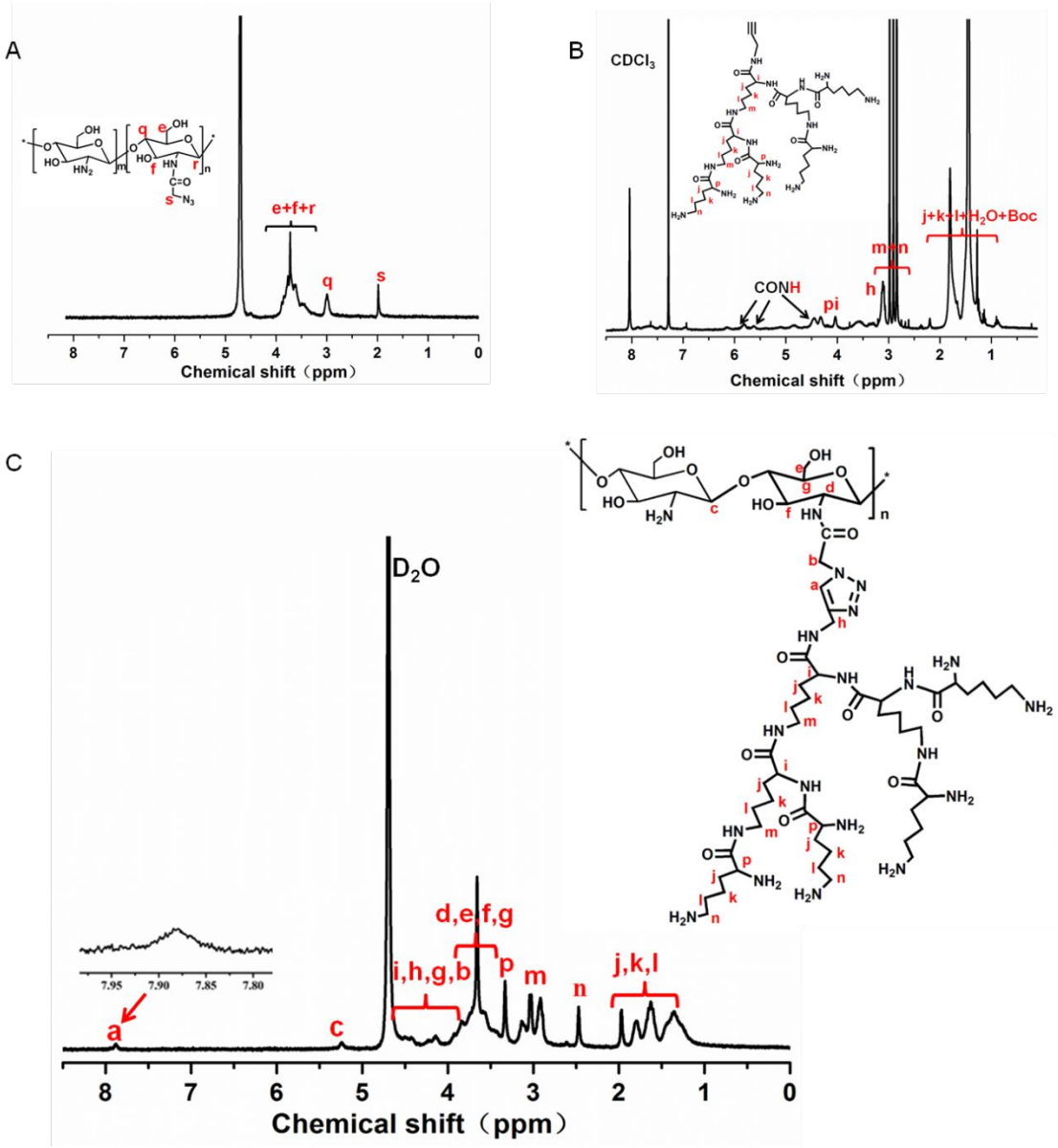

Figure S3. FTIR spectra of CS-N_3, alkynyl-PLLD-G_3 and CPL. FTIR Spectrum of CS-N_3 displayed a typical peak at 2100 cm^{-1}. Disappearance of this typical peak indicated the successful synthesis of CPL.

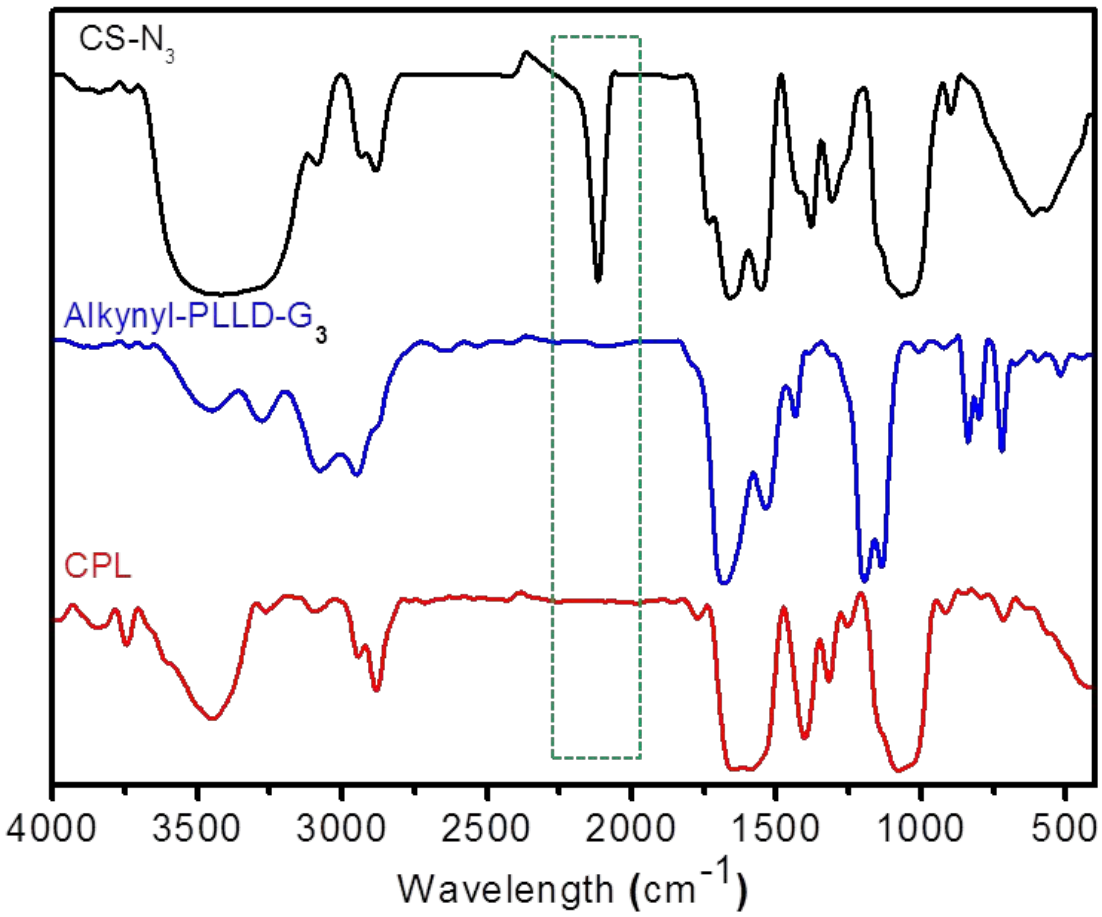

Figure S4. TEM (A) and size distribution (B) of Au-CPL NPs synthesized in the first 10 min. Au@CPL NPs displayed a spherical shape with a small size at about 7.3 ± 0.4 nm.

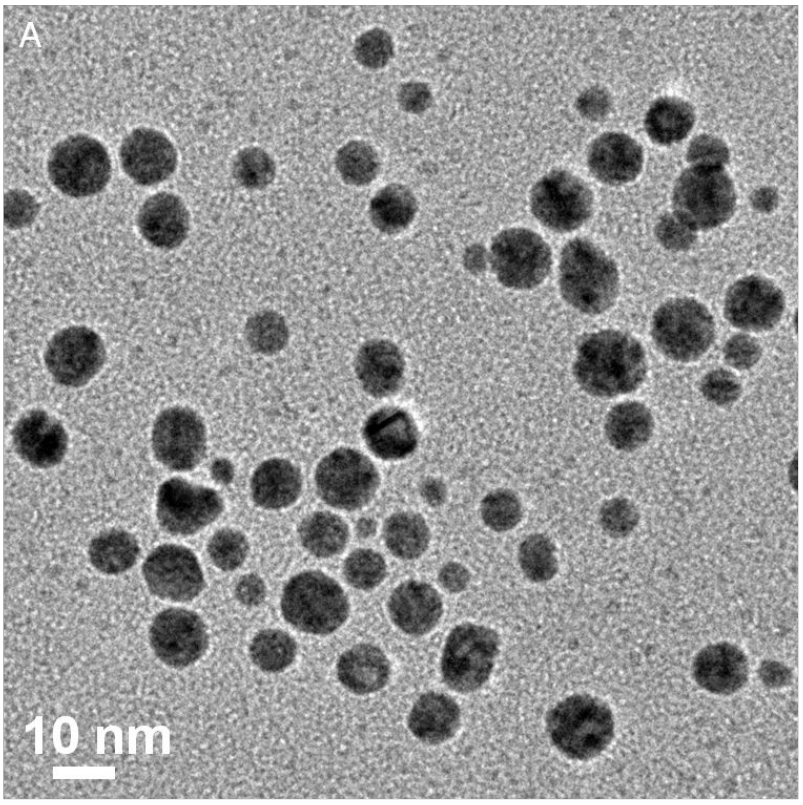

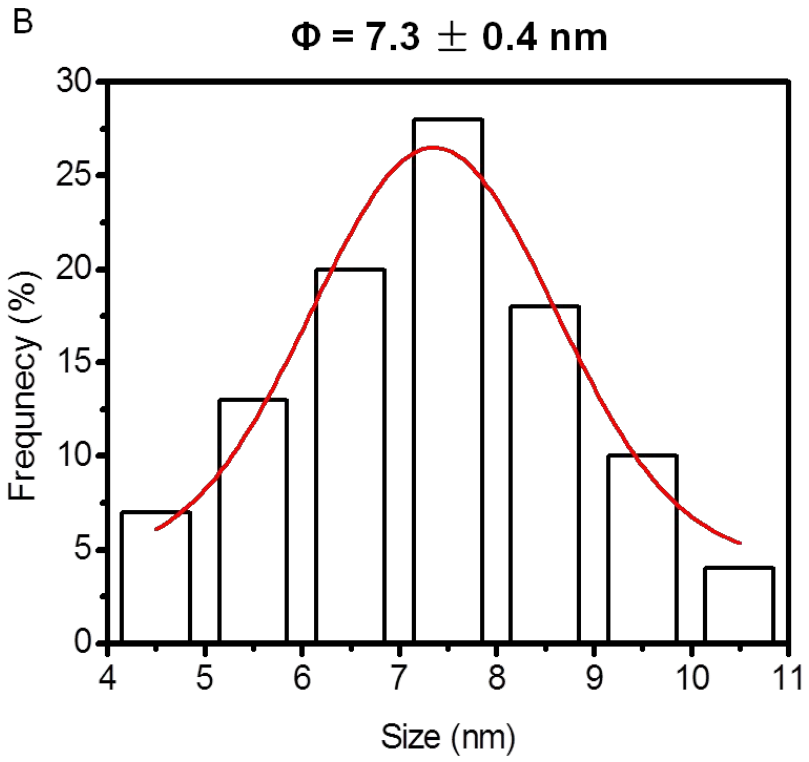

Figure S5. CT images of individual Au NPs (8 nm) and iohexol (Omnipaque) with different concentrations.

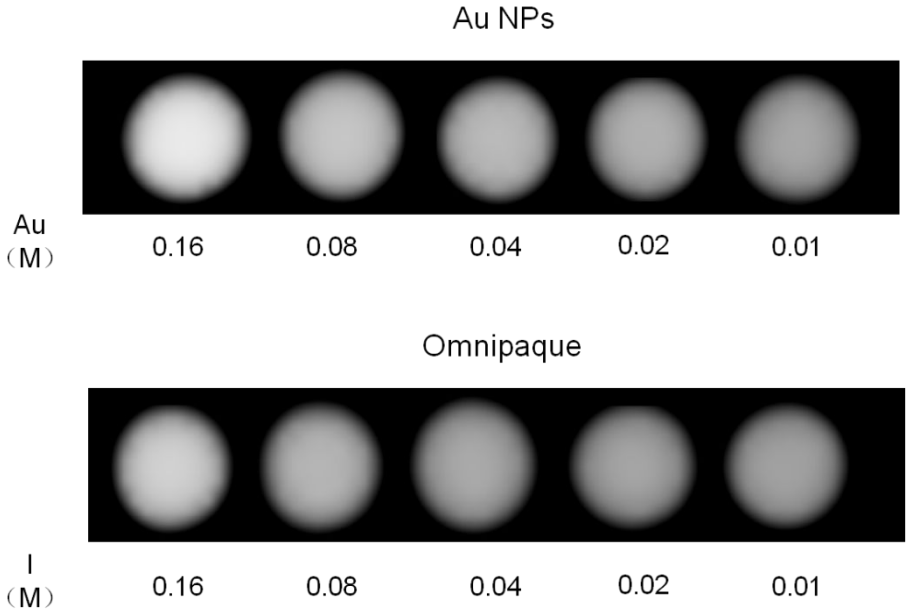

Figure S6. Cytotoxicity of Au@CPL-RGD and PEI with different concentration on MCF-7 cells. Concentration of 80, 120, 160, 200, 240 and 320 μg/mL were equivalent to the weight of Au@CPL-RGD in Au@CPL-RGD/pMMP-9 complexes with N/P ratio of 20, 30, 40, 50, 60 and 80, respectively.

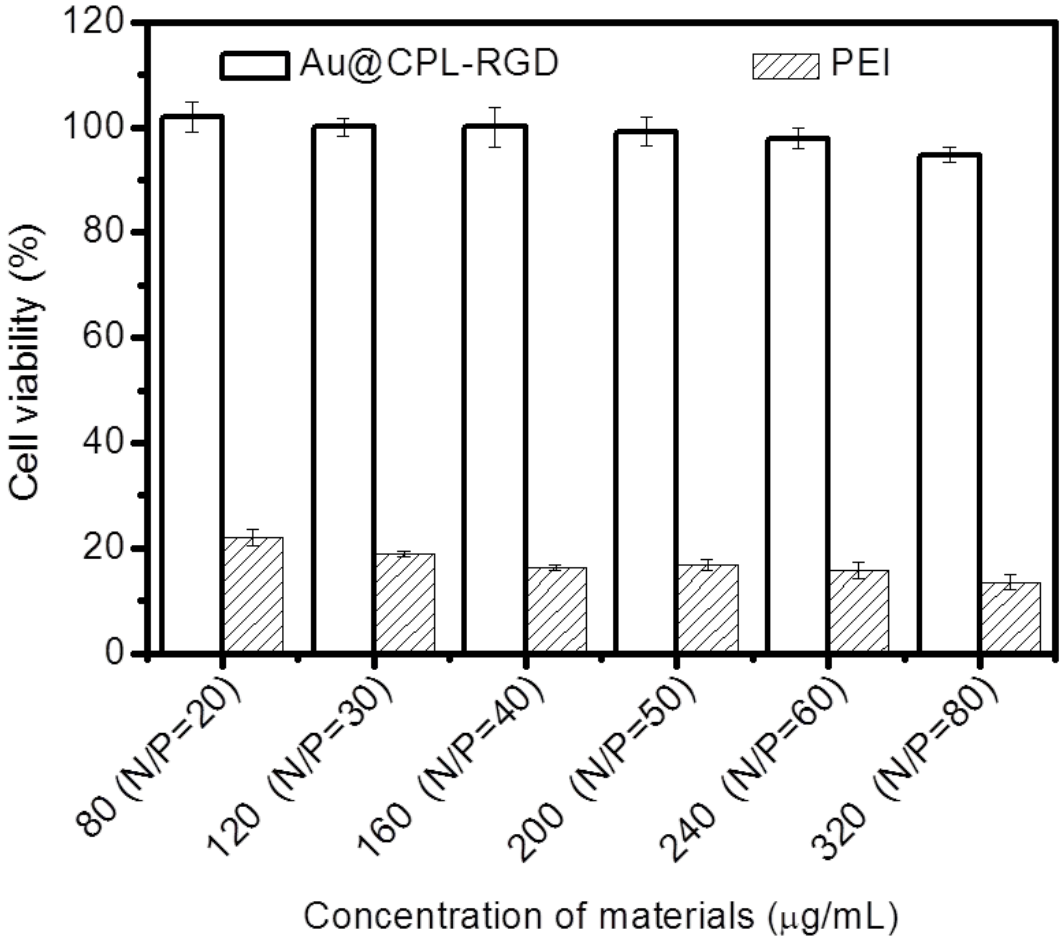

Figure S7. A, Fluorescent microscopic images showing the wound healing rate of cell gap under different treatment in 36h. B, Relative cell gap distance in different group after 36 h healing. Data presented as mean ± standard deviation, statistical significance was considered when $p<0.01$(***).

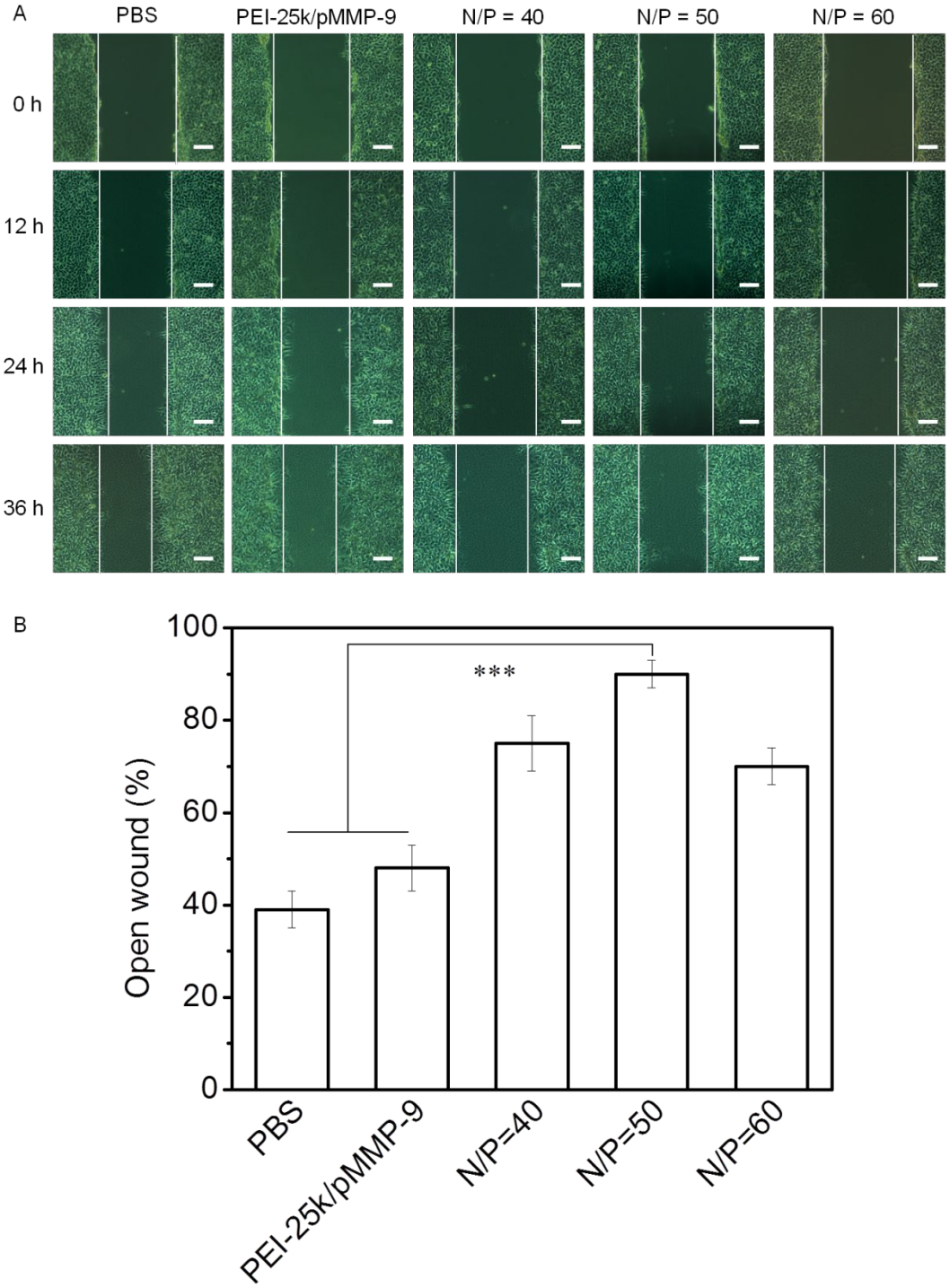

Figure S8. HU value determined from CT images of the tumor after intratumoral (*i.t.*) or intravenous injection (*i.v.*) of Au@CPL-RGD/pMMP-9. Data presented as mean ± standard deviation, statistical significance was considered when $p<0.01$(**) and $p<0.01$(***).

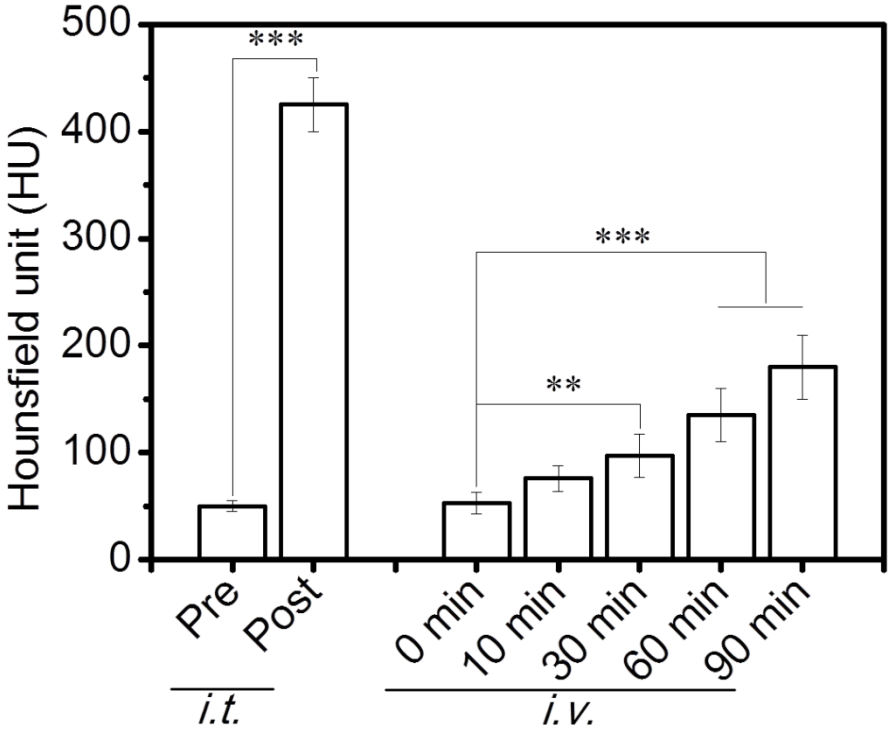

Figure S9. A, CT images of tumor-bearing nude mice after intravenous injection of Au@CPL/pMMP-9 complex at different times. B, changes in HU value determined from CT images of the tumor along with time.

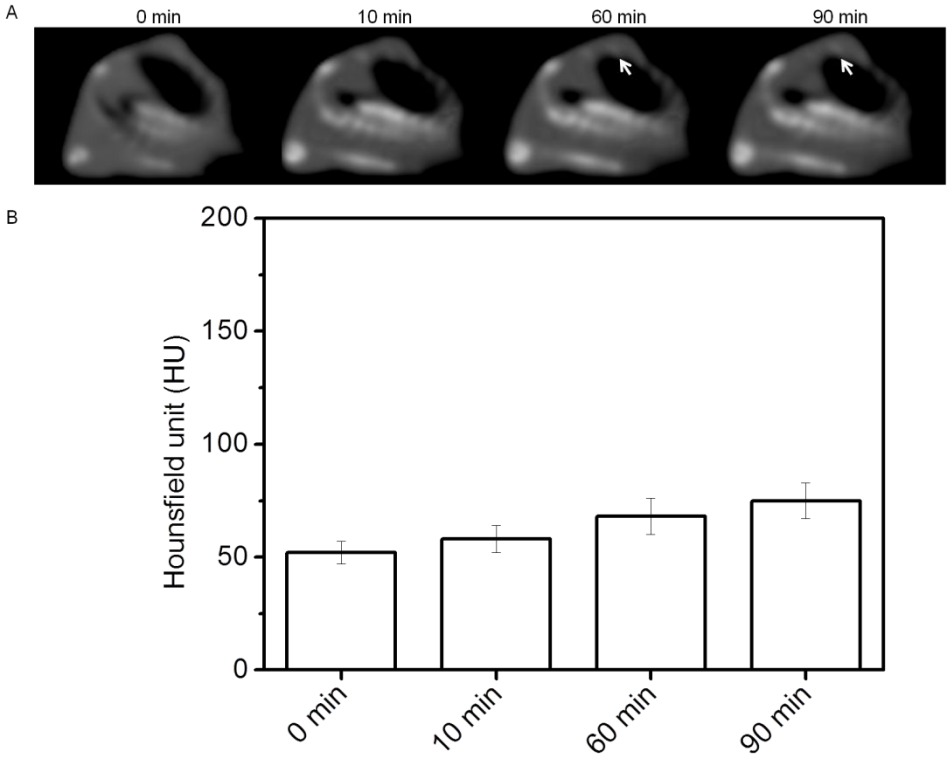

Figure S10. Images showing the tumor growth state in group of PBS, Au@CPL-RGD (*i.v.*), Au@CPL-RGD (*i.t.*) and Au@CPL-RGD/pMMP-9 (*i.v.*) at different days. It clearly showed that Au@CPL-RGD (*i.t.*) and Au@CPL-RGD (*i.v.*) did not have inhibitory effect on tumor growth, the size of tumor in those two groups were similar to that of the PBS control group.

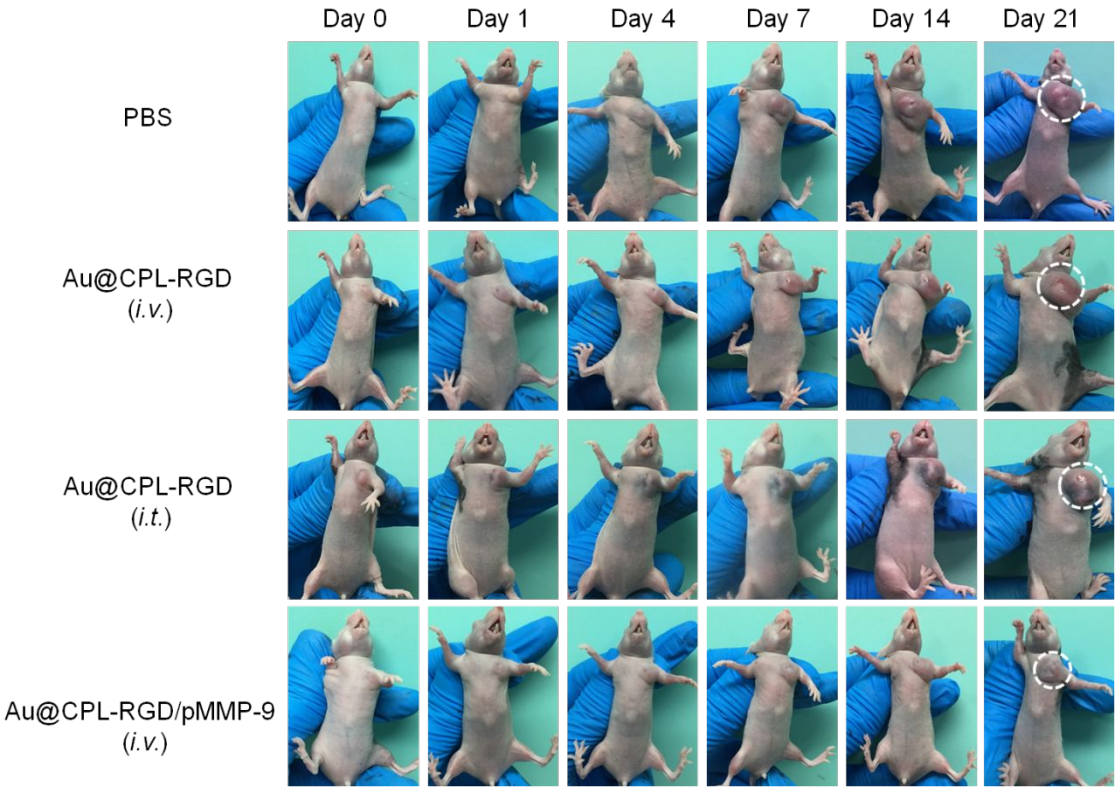

Figure S11. Changes in the mean body weight of mice in different treatment group in 21 days. a: PBS, b: intravenous injection of Au@CPL-RGD (*i.v.*), c: intratumoral injection of Au@CPL-RGD (*i.t.*), d: intravenous injection of Au@CPL-RGD/pMMP-9 (*i.v.*), e: intratumoral injection of PEI-25k/pMMP-9 (*i.t.*) and f: intratumoral injection of Au@CPL-RGD/pMMP-9 (*i.t.*).

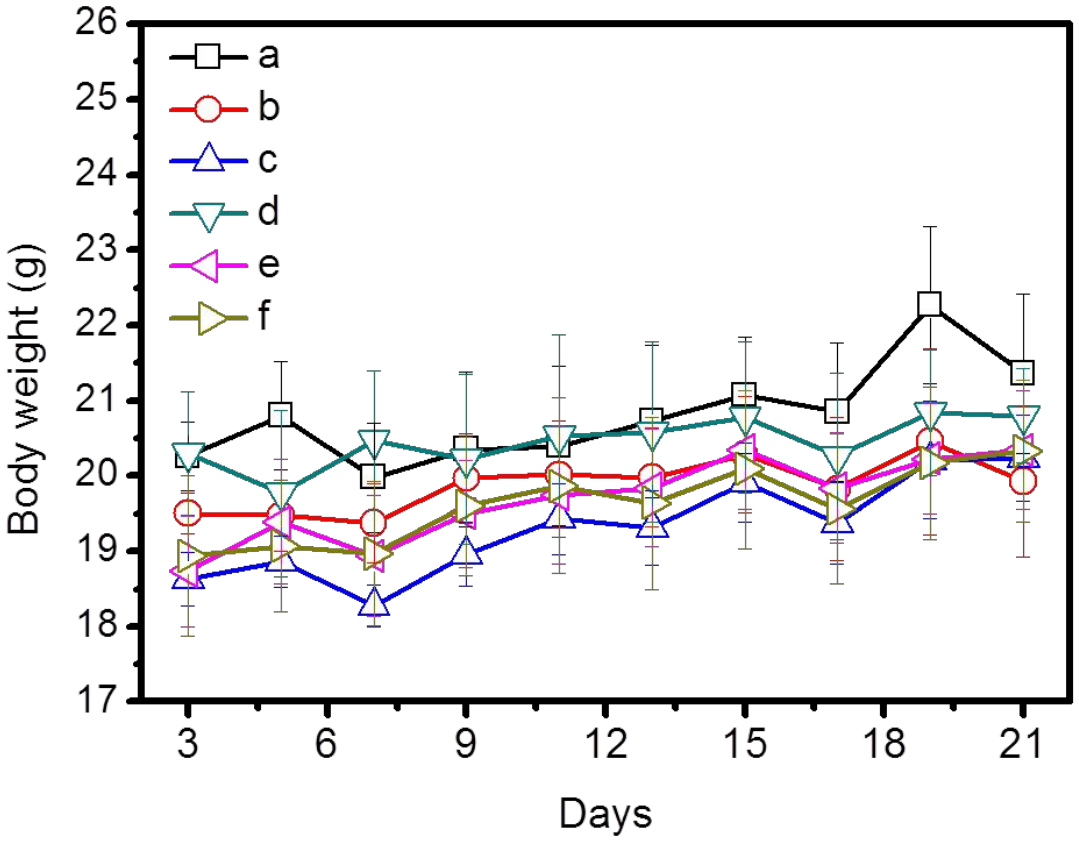

Figure S12. Slow ADC value determined from MRI images of different groups. Data presented as mean ± standard deviation, statistical significance was considered when $p<0.01$(**) and $p<0.01$(***).